Research Square

Preprints are preliminary reports that have not undergone peer review.
They should not be considered conclusive, used to inform clinical practice,
or referenced by the media as validated information.

Structural basis of ribosomal helix 69 modification by the pseudouridine N3-methyltransferase RlmH

Yong-Gui Gao

ygao@ntu.edu.sg

School of Biological Sciences, Nanyang Technological University https://orcid.org/0000-0001-7298-0835

Rya Ero

Nanyang Technological University

Xin-Fu Yan

Nanyang Technological University https://orcid.org/0000-0001-6248-2349

Joshua Yeo

School of Biological Sciences, Nanyang Technological University https://orcid.org/0000-0002-0253-0238

Phong Do

School of Biological Sciences, Nanyang Technological University

Aivar Liiv

University of Tartu

Suparna Sanyal

Uppsala University https://orcid.org/0000-0002-7124-792X

Jaanus Remme

University of Tartu https://orcid.org/0000-0002-4011-6580

Article

Keywords:

Posted Date: November 26th, 2026

DOI: https://doi.org/10.21203/rs.3.rs-11560585/v1

License: This work is licensed under a Creative Commons Attribution 4.0 International License.
Read Full License

Additional Declarations: There is **NO** Competing Interest.

Article

Structural basis of ribosomal helix 69 modification by the pseudouridine N3-methyltransferase RlmH

Ero Rya[1], Yan Xin-Fu[1], Yeo Yi Joshua[1], Do Phong Hoa[1], Liiv Aivar[2], Sanyal Suparna[3], Remme Jaanus[2*], Gao Yong-Gui[1*]

[1] School of Biological Sciences, Nanyang Technological University, Singapore 639798, Singapore

[2] Institute of Molecular and Cell Biology, University of Tartu, Tartu 51010, Estonia

[3] Department of Cell and Molecular Biology, Uppsala University, Uppsala 752 37, Sweden

[*]Corresponding authors. Email: jaanus.remme@ut.ee, ygao@ntu.edu.sg

Keywords: ribosome biogenesis, rRNA modification, helix 69 (H69), pseudouridine methylation, cryo-EM

Abstract

In all organisms, specific sets of nucleosides are post-transcriptionally modified during ribosome biogenesis. Helix 69 (H69) of the large ribosomal subunit lies near the decoding center, contributes to tRNA binding, interacts with translation factors, and forms the central intersubunit bridge B2a together with helix 44 of the small subunit. In *Escherichia coli*, H69 contains three RluD-dependent pseudouridine modifications at positions 1911, 1915, and 1917. Ψ1915 is further methylated at the N3 position by RlmH. Notably, RlmH is unique among ribosome modification enzymes because it targets pseudouridine and acts only on the 70S ribosome. The structural basis for this substrate specificity and the functional consequences of H69 modification remain unclear. Here, using cryo-electron microscopy, we examined H69 conformations in different ribosomal states and determined the structure of RlmH bound to the 70S ribosome. RlmH binds as a dimer to the ribosomal A-site region, contacting both subunits and remodeling H69 by flipping the substrate base into a composite active site formed at the dimer interface, accompanied by conformational changes in several RlmH residues. Curiously, RlmH binding also alters the conformation of the universally conserved H69 nucleotide A1913 and thereby perturbs the B2a bridge. Site-directed mutagenesis combined with *in vitro* and *in vivo* methylation assays identified conserved C-terminal residues, especially tyrosine-152, playing a critical role in positioning the substrate base for methyl transfer in the absence of a canonical general base. Finally, growth analyses indicate that H69 modifications contribute to bacterial fitness under stress conditions, consistent with a role in fine-tuning ribosome function.

Introduction

Ribosomes are complex ribonucleoprotein machines that catalyze protein synthesis in all cells. Post-transcriptional modification of ribosomal RNA (rRNA) is an integral part of ribosome biogenesis, and most modified nucleosides are positioned within, or close to, functionally important regions of the ribosome [1–3]. Despite their conservation and strategic locations, the biological roles of many rRNA modifications remain largely elusive.

Helix 69 (H69; also known as stem-loop 69) (Figure 1A) is a universally conserved element of the large ribosomal subunit (50S in bacteria). H69 lies near the decoding center, contributes to accurate translation, and participates in A- and P-site tRNA binding as well as interacts with translation factors. H69 residues also contact helix 44 (h44) of the small ribosomal subunit (30S in bacteria) to form the central intersubunit bridge B2a (Figure 1A). Consistent with these central functions, many H69 point mutations cause severe growth defects in *E. coli* by impairing translation [4].

A notable feature of H69 is its high content of modified nucleosides [5,6]. In *E. coli* 23S rRNA, H69 contains three modified positions: pseudouridines (Ψs) at 1911 and 1917 and N3-methylated pseudouridine ($m^3\Psi$) at position 1915 [1,7] (Figure 1A). All three H69 pseudouridines are generated by RluD [8]. Studies of free Ψ nucleoside indicate that the C-C glycosidic bond allows greater rotational freedom than the N-C glycosidic bond of uridine [9]. Using H69 model RNAs and biophysical approaches, Chow and co-workers showed that Ψ1915 and Ψ1917 destabilize the local H69 structure, whereas Ψ1911 has a stabilizing effect [10]. Overall, Ψs stabilize H69 under low pH conditions [11], enhance base stacking in H69 [12,13] , and provide an additional hydrogen-bond donor (Figure 1B), which can stabilize local RNA structure more effectively than uridine at the same position. Accordingly, Ψ1917, but not U1917, can form a non-canonical reversed Hoogsteen base pair with A1912, a universally conserved adenine nucleotide and a component of the intersubunit bridge B2a (Figure 1A) [14]. Ψ1911 is likely to make a similar reversed Hoogsteen interaction with A1919 (Figure 1A) [14]. The A1912 and Ψ1917 reversed Hoogsteen base pair is important for interactions between ribosomal subunits, implicating Ψ1917 as a modification involved in subunit association [14]. Consistent with this notion, ribosomes lacking H69 pseudouridines show reduced subunit association *in vitro* [15]. Although *rluD* is dispensable

under normal conditions, it becomes critical for rapid cell growth in bacteria with defects in translation termination [16,17].

N3 methylation of Ψ1915 modestly increases the thermodynamic stability of H69 model RNAs without substantially altering their overall structure [18,19]. Chow and co-workers proposed that Ψ1915 methylation may help stabilize specific long-range tertiary RNA-RNA or RNA-protein interactions [18]. However, its precise function in the context of ribosomes remains enigmatic. While deletion of *rlmH* has no notable effect on *E. coli* under optimal conditions, the mutant shows a clear growth disadvantage in competition with wild-type cells [20]. RlmH was identified as the methyltransferase that transfers a methyl group from the cofactor S-adenosyl-L-methionine (SAM) to the N3 atom of Ψ1915 in *E. coli* 23S rRNA [20,21] (Figure 1B). RlmH orthologs are widespread in bacteria [20–22]. Unlike most SAM-dependent RNA methyltransferases, which adopt an ancient Rossmann fold [23], RlmH belongs to the SPOUT (SpoU TrmD-like) methyltransferase superfamily, whose members are characterized by a deep topological knot and a homodimeric mode of action [22]. RlmH has remarkable substrate specificity: according to the MODOMICS RNA modification database [24], it remains the only known enzyme that methylates pseudouridine at the N3 position. RlmH does not methylate Ψ1911 or Ψ1917 in H69 [21], indicating that its substrate recognition mechanism differs from that of pseudouridine synthase RluD. In the absence of Ψ1915, RlmH is able to methylate the structurally related U1915, albeit inefficiently [25]. In wild-type cells, however, m^3U1915 is generally not detected [25], because RluD precedes RlmH action (Figure 1B). Indeed, RluD modifies nearly mature 50S subunits [25,26], whereas RlmH acts exclusively on 70S ribosomes [25]. A recent cryo-EM study has revealed RluD, with its catalytic aspartate-139 residue, is in close proximity to U1911 in H69 in the precursor 50S subunit [26].

The strict requirement for the 70S ribosome as a substrate is unprecedented among known ribosome modification enzymes and implies that the RlmH-dependent methylation is the very last constitutive modification introduced to rRNA during ribosome assembly. The specificity of RlmH for 70S ribosomes demonstrates that 50S maturation depends on the presence of 30S subunits, linking ribosome biogenesis to the onset of translation, given that subunit joining typically occurs during translation initiation. The translation initiation complex being the likely substrate of RlmH is in

agreement with the docking simulations of the RlmH crystal structure into the 70S ribosomes [20], which suggested that the RlmH dimer could bind near the ribosomal A site without interfering with mRNA or P-site tRNA, as would be expected for an initiation complex containing fMet-tRNA in the P site. These simulations further suggested that RlmH make extensive contacts with the small subunit while engaging the large subunit mainly through the H69 loop region [20]. Efficient methylation of Ψ1915 by RlmH likely requires the proper H69 conformation within the 70S ribosome [27]. By contacting both ribosomal subunits, RlmH resembles translation factors more than typical rRNA modification enzymes, which act during different stages of ribosome biogenesis: some modify nascent rRNA, others act on assembly intermediates, and still others, including RluD, modify nearly mature subunits [28]. Although crystal structures of apo RlmH (PDV: 1NS5) and RlmH bound to SAM or sinefungin (SAM analog, methyltransferase inhibitor) have been determined [29], the structure of RlmH in complex with the substrate 70S ribosome would illuminate how RlmH interacts with individual subunits as well as gains access to its substrate pseudouridine 1915 base in H69 and carries out the N3-methylation reaction.

As aforementioned, $m^3\Psi$1915 (*E. coli* numbering) in 23S rRNA is the only known example of $m^3\Psi$ modification in RNA, underscoring the unusual substrate recognition and methyl-transfer chemistry of RlmH. Nucleolar Essential Protein 1 (Nep1, named Emg1 in humans) is a SPOUT superfamily member that also methylates pseudouridine, albeit at the N1 atom of Ψ1191 (*S. cerevisiae* numbering) in yeast 18S rRNA [30,31]. The crystal structure of the *S. cerevisiae* Nep1 dimer bound to S-adenosyl-L-homocysteine (SAH, the methyl transfer product) and a short RNA oligonucleotide corresponding to the modification region in 18S rRNA demonstrated that Nep1 recognizes its substrate via base-specific interactions and that the substrate base is oriented in the active site for methyl group transfer from SAM to the N1 atom of substrate base [32]. Similarly, the SPOUT methyltransferase TrmY catalyzes methyl transfer to N1 of Ψ54 in archaeal tRNA [33], whereas RsmE modifies U1498 to m^3U in bacterial 16S rRNA [34]. Note that RlmH can synthesize m^3U1915 in the absence of Ψ1915, albeit inefficiently [21,25]. Structures of TrmY and RsmE bound to their RNA substrates are not yet available, leaving important questions about their substrate recognition mechanisms unresolved. Notably, RlmH and RsmE form antiparallel dimers [29], whereas Nep1 and TrmY adopt perpendicular dimer arrangements

[32,35]. Structural characterization of *E. coli* RlmH bound to its ribosomal substrate, therefore, offers an opportunity to clarify how different SPOUT methyltransferases recognize RNA and catalyze methyl transfer, including comparison with the well-studied tRNA m^1G37 TrmD [36]. To address these questions, we determined the atomic structure of *E. coli* RlmH in complex with the 70S ribosome and examined how amino acid substitutions in and around the catalytic site affect RlmH activity *in vivo* and *in vitro*.

Results

70S ribosome populations and the effect of H69 modifications

RlmH modifies Ψ1915, and, less efficiently, U1915 within H69 only in the context of the 70S ribosomes [21,25]. In accordance, we observed that purified recombinant RlmH, pre-incubated with the methyltransferase product SAH to stabilize enzyme-substrate complexes, co-pelleted through a sucrose cushion with 70S ribosomes isolated from either the *rlmH* single knockout strain (Δ*rlmH;* Ψ1911, Ψ1915, and Ψ1917 in H69) or the *rlmH* and *rluD* double knockout strain (Δ*rlmH/*Δ*rluD;* U1911, U1915, and U1917 in H69) (Figure S1). The recombinant RlmH carries an N-terminal His_6-tag, which did not measurably affect RlmH activity, whereas a C-terminal tag inactivated the enzyme. Removal of the N-terminal tag resulted in RlmH aggregation during purification. We therefore used N-terminally tagged RlmH for complex formation and applied the RlmH-SAH-70S(Δ*rlmH*) and RlmH-SAH-70S(Δ*rlmH/*Δ*rluD*) samples for cryo-electron microscopy (cryo-EM) analysis (Figure S2).

In both cryo-EM datasets, classification revealed three major RlmH-free ribosome states: vacant 70S particles, 70S particles with tRNA in the P-site and a corresponding mRNA density, and 70S particles containing both A- and P-site tRNAs together with mRNA density (70S, 70S+P, and 70S+AP, respectively; Figure S3). These populations allowed us to compare the effect of H69 modifications across distinct ribosomal states. In vacant 70S ribosomes, the overall conformation of unmodified H69 and the position of U1915 were like those observed in wild-type ribosomes containing native H69, although a small local shift was apparent (Figure S4A). More notably, in the unmodified H69, the A1913 base did not project into the minor groove of 16S rRNA h44 to engage A1492 and A1493, a key interaction within the B2a intersubunit bridge as seen with the native H69. The weaker electron density

for A1492 and A1493 is in line with partial disruption of B2a in ribosomes lacking H69 modifications. This effect is likely caused by the absence of H69 pseudouridines, foremost Ψ1917, whose non-canonical reversed Hoogsteen interaction with A1912 is important for interactions between the ribosomal subunits [14]. In agreement with this structural interpretation, ribosomes lacking H69 pseudouridines show reduced subunit association *in vitro* [15]

The base at position 1915 remained oriented toward the interior of H69 and stacked between C1914 and A1916, irrespective of the H69 modification state or the presence of tRNA(s) (Figure S4). By contrast, P-site tRNA binding affects the orientations of A1913, A1492, and A1493 differently in native and unmodified H69. In ribosomes with unmodified H69, A1913 was displaced from h44 and did not participate in B2a bridge interactions, unlike in ribosomes containing native H69 (Figure S4B). In native ribosomes with both A- and P-site tRNAs, A1913 in H69, together with A1492 and A1493 in h44, are rotated toward the A-site tRNA to make interactions with the anticodon region (Figure S4C). In this state, A1913 forms a hydrogen bond between its N1 atom and the 2'-hydroxyl group of ribose 37 in the A-site tRNA anticodon stem-loop [37]. Interestingly, the Δ*rlmH*/Δ*rluD* 70S+AP particles were classified into two sub-populations: in one, A1913 remained oriented toward h44 despite A1492 and A1493 flipping toward the A-site tRNA; in the other, A1913 adopted an A-site-facing orientation like that in the native ribosomes (Figure S4C). These observations suggest that H69 modifications, most likely the three pseudouridines, restrict the conformational dynamics of H69, particularly at A1913, and may thereby indirectly support A-site tRNA binding.

In the cryo-EM sample prepared from the Δ*rlmH*/Δ*rluD* cells, we also identified a population of 70S particles with additional density overlapping with the A-site region, consistent with a bound RlmH dimer (Figure 1C and S3). Interestingly, we did not detect RlmH-bound particles when ribosomes were prepared from the Δ*rlmH* strain. One possible explanation is that purified RlmH retains endogenous SAM, as often observed for methyltransferases, and can rapidly methylate Ψ1915 in Δ*rlmH* ribosomes, resulting in a more transient complex. By contrast, methylation of U1915 in Δ*rlmH*/Δ*rluD* ribosomes is less efficient, which may prolong the lifetime of the enzyme-ribosome complex and facilitate its capture. To test this, we repeated the experiment with methyltransferase inhibitor sinefungin

(SAM analog) and RlmH catalytic-site mutants (Y152A and E138A; discussed later). These attempts did not yield RlmH-bound Δ*rlmH* 70S particles, underscoring the dynamic nature of RlmH association with its ribosomal substrate.

Overall structure of the SAH bound RlmH in the ribosome

For the Δ*rlmH/*Δ*rluD* ribosome sample, we observed well-defined density for nearly the entire RlmH dimer, except for the ultimate C-terminal residue E155 facing H69 and the last three residues of the protomer whose C-terminus faces away from H69 (Figures 1C and S3). Additional density corresponding to the substrate base U1915 was located at the RlmH dimer interface, and SAH molecules were visible in both RlmH protomers, with one SAH positioned adjacent to the substrate base density (Figure 1D). The ribosome-bound RlmH structure was determined at ~2.2 Å resolution.

The structure shows that the RlmH dimer fits tightly into the ribosomal A-site region and makes multiple contacts with both the 50S and 30S subunits (Figure 2). This binding mode differs substantially from previous docking simulations, which predicted that most contacts would occur with the 50S subunit (Figure S5). The RlmH dimer does not overlap with P-site tRNA or the mRNA binding region (Figure S5), consistent with the possibility that RlmH could act on an initiation-like ribosome complex with initiator fMet-tRNA in the P-site. However, we did not observe any particles containing both RlmH and P-site tRNA (Figure S3). Similar results were obtained after *in vitro* reconstitution using purified RlmH, ribosomes, mRNA, and corresponding tRNA, as well as after nickel-affinity pull-down of His-tagged RlmH from *ΔrlmH/ΔrluD* cell lysate. Curiously, the pull-down approach yielded vacant 70S particles, 70S particles with P-site tRNA, and 70S particles containing RaiA protein (24% of particles), but no RlmH-bound ribosome population. Despite that we could not achieve structure of RlmH bound to 70S with P-site tRNA, an initiation-like complex cannot be excluded for RlmH substrate if it is too transient to be captured under our experimental conditions.

RlmH is the smallest known protein member of the SPOUT methyltransferases and lacks a separate RNA-binding domain [22,38]. Thus, ribosome recognition and substrate positioning are mediated by the core SPOUT domains of the two RlmH protomers. Overall, protomer A ($RlmH^A$) provides the

194 catalytically relevant cofactor-binding site, whereas protomer B ($RlmH^B$) contributes the C-terminal
195 region involved in substrate positioning and catalysis [29]. Both protomers contact H69 within the loop
196 region encompassing residues 1913-1917, which will be discussed in detail below. Outside H69, $RlmH^A$
197 interacts with the 50S subunit and $RlmH^B$ with the 30S subunit exclusively (Figure 2A). Compared with
198 the crystal structure of the SAM-bound RlmH dimer (PDB: 5TWJ) [29], substrate binding shifts the $RlmH^A$
199 loop region, comprising residues R43 to R51, toward H69 (Figure S6A). R43 likely stabilizes H69
200 binding by contacting the backbone of A1916, whereas L45 and R51 extend to interact with the
201 backbone phosphates of H71 residues C1962 and U1946, respectively. N46 is oriented towards the H71
202 major groove to establish interaction with the C1961 base O2 residue (Figure 2B). On the opposite side
203 of the H69 interface, $RlmH^A$ extends slightly to contact 23S rRNA H89 and the ribosomal protein L16
204 (Figures 2C and S6B). Specifically, R90 and R96 interact with the ribose 2′-hydroxyl groups of H89
205 nucleotides G2470 and A2482, respectively. In addition, the peptide backbones of D94 and G95 contact
206 the side chains of r-protein L16 residues R55 and R51, respectively.

207 In $RlmH^B$, K29 rotates upon substrate binding to interact with the backbone phosphate of the
208 h44 nucleotide A1493 (Figures 2D and S6C). Small conformational changes in N149 and P151 further
209 suggest that these residues contribute to 16S rRNA h44 binding. In addition, $RlmH^B$ contacts 16S rRNA
210 h18, including the phosphate backbones of C519 and A520, and ribosomal protein (r-protein) S12,
211 including T39 and L49, through the peptide backbones of D94 and G95, as well as the side chain of L93
212 (Figures 2E and S6D). On the opposite side of the protomer, positively charged $RlmH^B$ residues K11,
213 K42, R51, and K55 interact with the phosphate backbones of 16S rRNA residues U956 (h30), U958
214 (h30), G987 (h32), and U986 (h32), respectively (Figures 2F and S6E).

215 Apart from local rearrangements in the 23S rRNA H69 loop and the 16S rRNA h44 region
216 involved in bridge B2a and A-site tRNA binding, which are discussed below, RlmH binding does not
217 cause major changes in the 70S ribosome. Instead, the multiple contacts across both protomers described
218 above anchor the RlmH dimer at the subunit interface and orient its catalytic site facing the H69 substrate
219 loop (Figure 2A).

Cofactor binding site

Consistent with the crystal structures of RlmH bound to SAM or sinefungin [29], and with SPOUT-methyltransferase-cofactor complexes more generally [35], the two SAH molecules in our cryo-EM structure occupy pockets formed by the deep trefoil knots of the individual RlmH protomers. In both sites, SAH adopts the characteristic bent conformation, with the amino-acid moiety folded back toward the adenine base and the ribose in a 3'-*endo* conformation (Figure S7 A and B). The knotted architecture of SPOUT methyltransferases enforces this bent SAM/SAH conformation and positions the transferable methyl group optimally relative to the substrate [35]. By contrast, Rossman-fold methyltransferases typically bind SAM in an extended conformation, with the ribose adopting a 2'-*endo* conformation [23].

While the adenine moiety of SAH is buried deeply within RlmH, the methyl group position corresponding to SAM remains solvent-exposed and directed toward the substrate base. The cofactor-binding site is nearly identical to that observed in the RlmH-SAM crystal structure [29]. Residues L72, S121, and L122 form the adenine-binding pocket, whereas D73, G103, and G107 help accommodate the ribose moiety of SAH/SAM (Figure S7C). Cofactor recognition is mediated mainly by backbone interactions and hydrophobic side chains, including L72 and L122, a binding mode also seen in TrmD-SAH and Nep1-SAH crystal structures [32,39]. Notably, although both protomers bind cofactor, only one cofactor-binding site, shown here in $RlmH^{A}$, is positioned to participate directly in catalysis.

RlmH dimerization

Dimerization is a common feature of SPOUT methyltransferases and enables the cofactor-binding pocket of one protomer to be positioned next to catalytic residues of the second protomer. The two dimerization helices from each protomer can associate either in a perpendicular arrangement, as seen mainly in SPOUT enzymes that methylate ribose 2'-O positions, such as TrmH and RlmB, or in an antiparallel arrangement, which is more typical of base-methylating enzymes such as TrmD (m^1G) and RsmE (m^3U) [22,35]. RlmH follows the latter pattern, forming an antiparallel dimer (Figure S8A), whereas the pseudouridine N1-specific methyltransferases Nep1 and TrmY form perpendicular dimers [35].

The dimerization interface of ribosome-bound RlmH-SAH is nearly identical to that observed in the RlmH-SAM crystal structure and buries ~13% of the total surface area of each protomer [29]. W15 protrudes from the helix of one protomer, with its side chain stacking against the antiparallel helix of the other protomer, whereas the Y23 side chains face one another across the protomer interface (Figure S8B). V134 and L131 residues likely provide additional stabilization through cross-protomer hydrophobic interactions between the second pair of antiparallel helices. Thus, ribosome binding preserves the canonical antiparallel RlmH dimer while positioning the two protomers to form a composite catalytic site at the dimer interface.

RlmH-dependent conformational changes in ribosome H69/h44 region

Substrate binding and recognition by RNA modification enzymes are dynamic processes that often require coordinated conformational changes in both the enzyme and the RNA substrate, particularly when the target nucleotide is buried within a structured RNA element. As discussed above, the base at position 1915 is normally oriented toward the interior of H69, where it stacks between neighboring bases. This conformation is observed in ribosomes isolated from wild-type cells and from Δ*rlmH* (Ψ1911, Ψ1915, and Ψ1917 in H69) or Δ*rlmH*/Δ*rluD* (U1911, U1915, and U1917 in H69) cells, irrespective of A- or P-site tRNA occupancy (Figure S4).

The Δ*rlmH*/Δ*rluD* ribosome-bound RlmH structure reveals that enzyme binding flips the target base U1915 out of H69 and into the catalytic pocket, where it faces the SAH molecule (Figure 3A and B). Such base flipping is a common mechanism used by RNA methyltransferases and is also observed in the yeast Nep1-SAH complex bound to a short RNA corresponding to the substrate region in small ribosomal subunit [32] and in *Haemophilus influenzae* TrmD-sinefungin bound to tRNA [36]. RlmH binding also produces a pronounced rearrangement of A1913. In vacant 70S ribosomes with unmodified H69, A1913 is oriented toward h44 but does not participate in the B2a bridge interactions with A1492 and A1493 (Figure S4A). Upon RlmH binding, both A1913 in H69 and A1493 in h44 shift substantially, placing A1913 between A1493 and RlmH (Figure 3B). These H69/h44 rearrangements are stabilized by positively charged residues in RlmH^{B}, including R25, R26, and K29, which contact the rRNA backbone (Figure 3B). The overall orientation of unmodified A1913 in the RlmH-bound structure resembles that

seen in native ribosomes containing A- and P-site tRNAs (Figure S9), although RlmH does not induce the full A1492/A1493 rotation observed during A-site tRNA engagement.

Previous H69 mutagenesis studies showed that substitutions at A1912 and A1919 severely affect RlmH activity, whereas mutations at the neighboring C1914 and A1916 bases have more modest effects on Ψ1915 methylation [27]. Since mutations at A1919 and, to a lesser extent, A1912 affect ribosome subunit association, which in turn can slow down RlmH function, the previous experiments [27] were carried out in the presence of 20 mM magnesium ions, strongly stabilizing ribosome subunit interaction. Our structure provides a mechanistic explanation for these observations. Apart from the flipped target base at position 1915, discussed below, RlmH interacts mainly with the sugar-phosphate backbone of the H69 loop rather than making extensive base-specific contacts (Figures 2B and 3B). RlmH appears to recognize a particular conformational state of H69, with backbone geometry and local RNA dynamics playing central roles in substrate selection. This mode of recognition contrasts with that of Nep1, which recognizes a defined consensus sequence at its rRNA target site and forms several base-specific interactions that stabilize the bound RNA stem-loop [32]. Taken together, these observations suggest that RlmH binding presumably provides the energy needed to remodel H69/h44 and that RlmH exploits intrinsic H69 dynamics to select U/Ψ1915. This structural mechanism explains why RlmH modifies position 1915 but not Ψ1911 or Ψ1917 within the same H69 loop [21].

Conformational changes in RlmH catalytic site upon substrate binding

Substrate binding is accompanied by local rearrangements in the catalytic site of RlmH. Namely, the H129 residue in $RlmH^A$ and the C-terminal residues Y152, H153, and R154 in $RlmH^B$ undergo conformational changes to form interactions with the RNA compared with those in the RlmH-SAM crystal structure [29] (Figure 3C). Indeed, this observation rationalizes why the addition of an affinity tag to the RlmH C-terminus completely inactivated the enzyme in our initial test. Unlike the SAM- and sinefungin-bound crystal structures, in which the C-terminal residues form a short helix, the corresponding region in the present structure (with the substrate ribosome and SAH bound) is more extended and resembles the apo RlmH conformation (Figure S7B). In the SAM- or sinefungin-bound structure [29], $RlmH^B$ H153 forms a hydrogen-bonding interaction with the hydroxyl group of S145,

stabilizing the short C-terminal helix. In the ribosome-bound structure, however, H153 rotates away from S145 and toward U1915 (Figure 3C). Thus, the RlmH-SAH-ribosome complex likely captures a relaxed post-methyl-transfer state preceding substrate release.

RlmH catalytic site and pseudouridine N3-specificity

In line with the complex representing a post-methyltransfer state, the distance from the target atom at position 1915 (N3 in pseudouridine or C5 in uridine) to the methyl group position in SAM is 4.9 Å (Figure 3D and Figure S10 A and B), and the distance to the sulfur atom in SAH is 5.7 Å. For comparison, the corresponding distance in the Nep1-SAH-RNA structure (PDB: 3OIJ) is 4.4 Å [32] (Figure S9C). We cannot rule out the possibility that U1915 in unmodified H69 adopts a slightly different conformation from Ψ1915, particularly given that pseudouridines have been shown to affect H69 dynamics as aforementioned. Nevertheless, RlmH can methylate ribosomes containing U1915 [21,25], indicating that the present complex with *ΔrlmH/ΔrluD* ribosomes represents a catalytically relevant state.

In the catalytic site, the flipped U1915 base is stabilized by interactions of its O2 atom with $RlmH^A$ H129 and O4 atom with $RlmH^B$ R142 (Figure 3D). In addition to supporting substrate binding and recognition, these interactions may help facilitate N3 deprotonation by stabilizing negative charge that develops during the reaction. Furthermore, the substrate base also stacks against $RlmH^B$ Y152 (Figure 3D). Notably, the Y152 hydroxyl group lies 3.7 Å from C5 of U1915, which corresponds to N1 in pseudouridine, suggesting that Y152 contributes to discrimination between uridine and pseudouridine. A hydrogen bond between Y152 and N1 of pseudouridine could further stabilize the preferred substrate, providing a structural explanation for the lower efficiency of RlmH-dependent methylation on ribosomes containing U1915 [21]. The U1915 nucleoside is additionally stabilized by the interaction between its ribose 2' O and the side chain of R154, which in turn interacts with E106 (Figure 3D). Together, these interactions form a local network of interactions that positions the substrate nucleotide in the catalytic site.

Recognition of the target atom within the substrate nucleotide is closely linked to the chemistry of methyl transfer. The orientation of the flipped base determines which atom is positioned for

nucleophilic attack on the reactive methyl group of SAM. Like Nep1, RlmH lacks a conventional general base that could abstract a proton from the target atom before methyl transfer (Figure S10 B and C), a catalytic strategy used by several SPOUT methyltransferases, including TrmD, whose D169 residue acts as a general base [22,35] (Figure S11). While the ultimate C-terminal E155 could not be modeled, it is unlikely to serve as a general base, given that it is poorly conserved and absent in some RlmH orthologs. To clarify the catalytic mechanism, we next carried out site-directed mutagenesis to identify RlmH residues required for Ψ1915 methylation in the *E. coli* ribosome both *in vivo* and *in vitro*.

In vivo methylation of ribosome by RlmH

To test the functional importance of residues identified from the structure, we selected ~12% of RlmH amino acids for mutagenesis based on sequence conservation and proximity to SAH and U1915 in our structure. In most cases, alanine substitutions were introduced to eliminate side-chain functionality while minimizing the conformational flexibility associated with glycine. The activity of each variant was assessed by monitoring Ψ1915 methylation in an *E. coli rlmH* deletion strain (*ΔrlmH*) expressing plasmid-encoded RlmH proteins. We took advantage of low basal transcription from the araBAD promoter in the absence of arabinose [20,21,40] to maintain low intracellular RlmH levels and thereby reveal activity defects in the variants. 70S ribosomes were isolated from cells at different growth phases (OD_{600} 0.3-2.4; Figure 4A), a design that effectively varied the substrate-to-enzyme ratio. During early to mid-log phases, active ribosome synthesis produces a high ribosome precursor pool and a low enzyme/substrate ratio [41]. In late log phase, ribosome synthesis decreases by approximately two orders of magnitude [42], whereas basal RlmH expression is expected to remain relatively constant, increasing the effective enzyme/substrate ratio. To further test whether activity defects could be overcome by higher enzyme levels, late log phase cells (OD_{600} ~2.5) were also analyzed after moderate arabinose induction (0.002%) (Figure 4B). rRNA was extracted from purified 70S ribosomes and analyzed for methylation at position 1915 by primer extension, as described in materials and methods. N3 methylation of Ψ1915 disrupts Watson-Crick base pairing and leads to a strong reverse transcriptase stop; the resultant cDNAs were separated by denaturing polyacrylamide gel electrophoresis (PAGE)

(Figure 4A). Subsequently, bands corresponding to the stop signal caused by $m^3\Psi$1915 were quantified (Figure 4B).

Plasmid-encoded wild-type RlmH methylated Ψ1915 efficiently even during the early exponential phase, indicating that the expression level was comparable to that of native RlmH (Figure 4A). In late log phase *ΔrlmH* cells, the level of $m^3\Psi$1915 was similar under low basal expression and moderate arabinose induction (~70%; Figure 4B), in line with previous reports [21,25]. All RlmH substitutions reduced methylation activity relative to wild-type RlmH (Figure 4A and B). Of note, the L127A and R142L mutations likely caused RlmH misfolding or destabilization, as these proteins could not be purified successfully in subsequent experiments. Among all tested variants, only Y152A completely abolished enzymatic activity. By contrast, Y152F retained detectable methylation when expressed at higher levels, consistent with our structural data that Y152 stacks against the substrate base (Figure 3D).

Under low-expression conditions in the early exponential phase, the RlmH variants Y23, E56, E106, G107, E138, and R154 showed little or no detectable methylation activity (Figure 4A). Upon arabinose induction, these variants regained detectable methylation at position 1915 (Figure 4 A and B), indicating that the corresponding residues strongly affect catalysis and/or substrate while not being absolutely required for activity. Together with the complete loss of activity in Y152A, these results identify Y23, E56, E106, G107, E138, Y152, and R154 as important contributors to RlmH function. Among them, G107, E138, R142, and Y152 are universally conserved [21]. In contrast, mutations L72A, D73A, G103A, S121A, L122A, T126A, P128A, H129A, Y141A, R142A, R142K, and H153A had more limited effects on Ψ1915 methylation (Figure 4 A and B). The very low activity of R142L is likely attributed to protein misfolding, as the other substitutions (R142A and R142K) retained methylation activity at low expression levels (Figure 4). These *in vivo* data are consistent with our structure: L72, D73, G103, G107, S121, and L122 are involved in SAM binding predominantly through backbone-mediated interactions (Figure S7C), whereas E106, H129, E138, R142, Y152, H153, and R154 are positioned near U1915 and contribute to substrate binding or positioning (Figure 3 D). In addition, the residues Y23 (Figure S8) and P128 (positioned at the interface) contribute to methylation by stabilizing

the RlmH dimer. As for the residues E56, T126, and Y141, it appears that they are too far away from the substrate and cofactor, suggesting that they contribute indirectly by maintaining an optimal catalytic-site architecture. None of the mutations tested detectably reduced RlmH specificity for Ψ1915, as m^3U1915 formation in the *rlmH/rluD* double-deletion strain was not increased relative to wild-type RlmH.

In vitro methylation of ribosome by RlmH

To further investigate the role of the residues identified above, we characterized the *in vitro* activity of native and mutant RlmH proteins by determining their kinetic parameters. The RlmH Y152A variant can be successfully purified but was not included in the kinetic analysis, as the mutation completely abolishes catalytic activity in the *in vivo* assay. Moreover, the L127A and R142L variants were excluded because they were unstable during purification.

The apparent K_M and k_{cat} values for 70S ribosomes and SAM were determined using purified RlmH proteins and radiolabeled SAM, following the assay established for native RlmH [25]. For 70S ribosomes, initial rates were measured at high SAM concentration (100 μM) over a range of 70S ribosome concentrations; for SAM, initial rates were measured at 2 μM ribosome concentration over a range of SAM concentrations. RlmH-dependent incorporation of [^{3}H]-methyl groups into ribosomes was monitored by trichloroacetic acid (TCA) precipitation followed by scintillation counting. The apparent K_M and k_{cat} values were estimated by fitting the initial-rate data to the standard Michaelis-Menten equation and are summarized in Table 1. Values represent the average of two experiments. For wild-type and G107A, the k_{cat} values determined using either 70S ribosomes or cofactor SAM as the varied substrate agreed well, differing by less than 20%, indicating that the kinetic measurements were obtained under appropriate conditions. Previously reported [25] kinetic parameters for native untagged RlmH are also included in Table 1 and are similar to those reported for N-terminal His-tagged RlmH by Koh et al., [29]. The ~1.6-fold difference in K_M, and consequently in kcat/K_M, for 70S ribosomes between the present and previous studies is likely attributable to differences in ribosome preparation. Therefore, ribosomes from the same preparation were used throughout the current kinetic study.

The *in vitro* methylation data support roles of RlmH residues L72, D73, G103, G107, S121, and L122 in SAM binding (Table 1). Among these, the G107A mutation has the strongest effect on both K_M and k_{cat}, consistent with the *in vivo* methylation results (Figure 4). Overall, however, the effects of mutations in the cofactor-binding pocket are relatively modest, supporting the structural observation that most SAM contacts are mediated by the RlmH peptide backbone rather than by side-chain-specific interactions. The kinetic parameters further indicate that E106, E138, R142, Y152, R154 and, to a lesser extent, H129 and H153, contribute to substrate-base binding, stabilization, or positioning within the catalytic site. These findings agree well with the *in vivo* data and with the structural arrangement of these residues around the flipped U1915 nucleotide (Figure 3D and Figure 4).

The catalytic mechanism by RlmH

The ribosome-bound RlmH structure, together with the *in vivo* and *in vitro* methylation data, identifies Y152 as a central residue for substrate-base stabilization. Y152 stacks against the U1915 base and is essential for productive catalysis: replacement with alanine completely abolished RlmH activity, whereas substitution with another aromatic acid, phenylalanine, caused a strong but incomplete loss of activity (Figure 3D, Figure 4, and Table 1). The Y152F substitution specifically tests the contribution of the tyrosine hydroxyl group, which interacts with the side chain of R142 that, in turn, forms a salt bridge with E138 (Figure 3D). Curiously, Koh et al. reported complete loss of activity for Y152F without impaired ribosome binding and proposed that Y152, potentially with a perturbed pK_a in its structural context, could act as a general base, analogous to catalytic tyrosines in SET-domain lysine methyltransferases [29]. Our data argue instead that Y152 primarily stabilizes and positions the substrate base. Given that Y152 faces the N1 side of pseudouridine, rather than the N3 atom that must be deprotonated, and Y152F retains residual methyltransferase activity, thus the N3 proton is more likely accepted by a water molecule, as discussed below. By facing the N1/C5 side of pseudouridine or uridine, Y152 may also contribute to substrate discrimination, consistent with the lower efficiency of RlmH-dependent methylation on ribosomes containing U1915 [21]. However, neither Y152A nor Y152F detectably increased m^3U1915 formation in the *rlmH/rluD* double deletion strain compared with wild-

type RlmH. Thus, in cells, the sequential action of RluD followed by RlmH likely provides the principal safeguard that ensures proper H69 modification during ribosome biogenesis.

R142, which corresponds to a functionally important residue R154 in TrmD (Figure 11 B and C), also contributes to substrate-base engagement. However, whereas the equivalent alanine substitution completely inactivates TrmD [39], RlmH retained partial activity upon mutation of R142. Direct hydrogen bonding between R142 and the substrate base is unlikely to be the dominant determinant of activity, because R142K and R142A had similar effects on RlmH function (Figure 4 and Table 1), whereas R142L likely destabilized the protein and impaired folding. These observations suggest that R142 mainly supports the catalytic architecture by stabilizing Y152 through its interaction network with E138 (Figure S10), which nicely rationalizes the strong negative effect of E138A mutation in both *in vivo* and *in vitro* assays (Figure 4 and Table 1). Consistent with this view, Koh et al. reported reduced or abolished *in vitro* methylation activity for RlmH R142 and E138 variants, respectively, without evidence that E138A or E138Q compromises ribosome binding [29].

Substrate binding also induces notable conformational changes in H129, H153, and R154 (Figure 3C). Alanine substitution of these residues caused moderate defects for H129A and H153A and a stronger defect for R154A in both *in vivo* and *in vitro* assays (Figure 4 and Table 1). Koh et al. similarly reported no detectable *in vitro* activity for H153F and R154A, and the latter exhibited compromised ribosome binding [29]. In our structure, the penultimate R154 stabilizes the substrate nucleotide by contacting the ribose 2′-hydroxyl group at position 1915 (Figure 3D). The substrate-induced repositioning of H153 and R154 in $RlmH^{B}$ is further stabilized by an interaction between R154 and E106 from the $RlmH^{A}$ protomer (Figure 3C and D), providing a structural explanation for the effect of E106A (Figure 4 and Table 1). H129 in $RlmH^{A}$ also shifts substantially upon substrate binding and faces the O2 atom of the uridine/pseudouridine base, where it may help stabilize charge redistribution during methyl transfer. This positioning is consistent with the moderate effect of H129A observed here and previously (Figure 4, Table 1, and ref. [29]). Together, these data support a mechanism in which Y152, R142, E138, H129, E106, H153, and R154 cooperate to stabilize the flipped substrate nucleotide and

organize the active site, while deprotonation of N3 is most likely mediated indirectly, potentially through a water-assisted pathway.

Functional role of H69 modification

The stabilizing effect of H69 modifications has been examined mainly using H69 model RNAs. Our structural analysis of ribosomes with unmodified H69 shows increased conformational heterogeneity in the H69 and h44 regions (Figure S4), which are central to the formation of the B2a intersubunit bridge and to tRNA binding. Although deletion of *rluD* causes little growth defect under normal conditions, it becomes important for rapid growth when translation termination is impaired [16,17]. Similarly, deletion of *rlmH* has only a negligible effect on *E. coli* growth under optimal conditions but confers a clear disadvantage in competition with wild-type cells [20]. Furthermore, RlmH overexpression has also been associated with enhanced ethanol tolerance [43]. Like the majority of the 23S rRNA modification enzymes [51], RluD and RlmH, and/or the corresponding modifications likely confer a fitness advantage under stress conditions. To assess the physiological contribution of H69 modification, we measured the doubling times of the *rlmH* single-knockout strain, which retains Ψ1911, Ψ1915, and Ψ1917, and the *rlmH/rluD* double-knockout strain, which lacks all three H69 modifications, under suboptimal growth conditions and compared them with wild-type *E. coli* (Figure 5).

Deletion of *rlmH* alone or together with *rluD* caused only a modest increase in doubling time at 37 °C in rich medium, but the growth defects became more apparent at suboptimal temperatures (Figure 5A). Increased doubling times were also observed at suboptimal pH in rich medium (Figure 5B) and were particularly evident in minimal media at pH 5 (Figure 5C). These effects were seen in both the *rlmH* single-knockout and the *rlmH/rluD* double-knockout strains, indicating that both Ψ1915 methylation and H69 pseudouridylation contribute to bacterial fitness during cold and pH stress. By contrast, high salt stress (0.5 M NaCl) and low-magnesium stress induced by EDTA did not measurably alter the doubling times of the mutant strains relative to wild-type cells (Figure 5D).

The SPOUT methyltransferases TsnR and AviRB have been linked to antibiotic (i.e., avilamycin and thiostrepton) resistance [44,45]. The tuberactinomycins viomycin and capreomycin are known to bind

at the ribosomal subunit interface near the intersubunit bridge B2a and block translocation during protein synthesis [46]. These drugs have been used in cryo-EM studies to stabilize transient ribosome conformations and improve conformational homogeneity. Superimposing the ribosome-bound viomycin and capreomycin structures [46] to 70S ribosomes with unmodified H69 and both A- and P-site tRNAs reveals that the drug binding site overlaps with the present A1913 position (Figure S12). Hence, H69 modifications, either directly or via their effects on conformational flexibility, may affect bacterial sensitivity to viomycin and capreomycin. Thus, we studied the effect of H69 modification on cellular sensitivity to viomycin and capreomycin.

The minimal inhibitory concentrations of viomycin and capreomycin for the *rlmH* and *rluD* single deletion strains were similar to wild-type *E. coli*. However, based on growth assays in the presence of 50 μg/ml viomycin or capreomycin, H69 pseudouridylation appears to affect the sensitivity of *E. coli* cells to these antibiotics (Figure 5D and Figure S13). This observation is in line with the binding of viomycin and capreomycin near H69 A1913 and h44 nucleotides A1492 and A1493 [46], a region whose conformation is affected by H69 modification status.

Discussion

In bacteria, most rRNA modifications are installed by dedicated enzymes that must both recognize a specific ribosomal substrate and catalyze a defined chemical reaction. These two processes are often coupled: energy from binding to the rRNA substrate can help drive substrate discrimination, local RNA remodeling, and catalytic activation [47]. Many rRNA modification enzymes therefore have modular architectures, with RNA-binding domains that target rRNA regions or assembly intermediates and catalytic domains that carry out the modification reaction. RlmH is an exception. It consists solely of the SPOUT methyltransferase core domain [22,35,45], and acts specifically on the 70S ribosome by binding at the interface between the two ribosomal subunits (Figures 1 and 2). In this respect, RlmH resembles a translation factor more than a typical rRNA modification enzyme. The RlmH-SAH-70S structure presented here shows how the RlmH dimer is anchored through contacts with both subunits, how H69 is remodeled to expose the substrate base, and how the composite catalytic site positions the substrate for methyl transfer.

RlmH does not undergo extensive global remodeling upon ribosome binding, consistent with structures of other SPOUT RNA modification enzyme complexes [32,36]. Instead, complex formation is accompanied by focused changes in the catalytic site and substrate RNA. The C-terminal residues Y152-E155, which form a short helix in the SAM-bound crystal structure [29], adopt a different conformation in the ribosome-bound complex and stabilize the flipped U1915 base in the catalytic pocket facing the cofactor-binding site (Figure 3C). Substrate base flipping, involving rotation around the flanking phosphodiester bonds, is a common strategy used by Rossmann-fold methyltransferases, SPOUT methyltransferases, and pseudouridine synthases [32,36,54–58]. In addition to flipping U1915, RlmH repositions A1913 in H69 and A1492/A1493 in h44, thereby perturbing the B2a intersubunit bridge (Figure 3 A and B). This is notable because A1913 acts as an important local pivot linking H69 conformation to translation control, tRNA engagement, and subunit interactions.

RlmH binding presumably provides part of the energy required to remodel H69 and h44, while also exploiting the intrinsic dynamics of H69 for substrate recognition. As the ability of RNA to adopt a certain conformation is encoded by both sequence and local structure, RlmH can achieve site selectivity with relatively few direct base-specific contacts, as revealed by our results (Figure 2B and 3B). This provides a structural explanation for why RlmH modifies position 1915 but not Ψ1911 or Ψ1917 within the same H69 loop [21]. It also helps rationalize previous H69 mutagenesis data: substitutions at A1912 and A1919 that via non-canonical reversed Hoogsteen base pairs interactions with Ψ1917 and Ψ1911, respectively, which influence the overall H69 architecture, strongly impair RlmH activity, whereas substitutions at the neighboring C1914 and A1916 bases have more modest effects on Ψ1915 methylation [27]. This mode of recognition contrasts with that of the $m^1\Psi$-specific methyltransferase Nep1, which recognizes a defined consensus sequence at its rRNA target site and stabilizes the bound RNA stem-loop through several base-specific interactions [32].

RlmH methylates U1915 in H69 less efficiently than the structurally related Ψ1915 [21,25]. The key distinction between pseudouridine and uridine is the presence of N1 nitrogen in pseudouridine, instead of the C5 carbon in uridine (Figure 1B). This feature on the flipped substrate base is oriented toward the universally conserved residue Y152 in RlmH, which, based on structural and mutagenesis

studies, forms a stacking interaction with the substrate base and is essential for efficient methyl transfer. While Y152 may therefore contribute to the preference for pseudouridine over uridine, the sequential action RluD followed by RlmH (Figure 1B) likely provides the major cellular mechanism that ensures correct H69 modification.

Regardless of its contribution to substrate selectivity, Y152 is clearly important for catalysis (Figure 4). Methyltransferases generally transfer the electrophilic methyl group of SAM directly to the substrate atom, a reaction that requires deprotonation of the target atom before or during methyl transfer. In many methyltransferases, the proton is accepted by a general base, such as D169 in TrmD [36]. RlmH, however, lacks an obvious residue positioned to serve this role (Figures S10 and S11). Koh et al. proposed that Y152 could act as a general base because its local environment might perturb its pK_a [29]. Although catalytic tyrosines are known in SET-domain lysine methyltransferases [29], comparable examples among RNA methyltransferases are not well established. Our data argue against Y152 acting as the principal general base: the Y152F variant, which lacks the hydroxyl group, retains residual Ψ1915 methylation activity upon moderate expression *in vivo* (Figure 4), and Y152 faces the N1 position of pseudouridine (C5 in uridine), rather than the N3 atom that must be deprotonated (Figure 3D). A related deprotonation problem has been discussed for the yeast N1-specific pseudouridine methyltransferase Nep1, where S233 was proposed to mediate proton transfer to the more distant (~6.3 Å) D101 (Figure S10C) [48]. In RlmH, E138, the structural counterpart of Nep1 D101, lies approximately 6.0 Å from the substrate deprotonation site and may therefore accept the proton from Y152 located midway and functioning as a mediator via its hydroxyl group (Figure S10B). However, unlike Y152A, E138A does not abolish RlmH activity completely (Figure 4 and Table 1), and its effect differs markedly from the strong catalytic defect reported for Nep1 D101A [48]. Mutagenesis of conserved and semi-conserved residues around the catalytic site instead highlights E106, R142, and R154 as important contributors to substrate positioning and active-site formation (Figure 4 and Table 1). In the structure, R142 contacts the substrate-base O4 atom, whereas E106 from the opposite protomer stabilizes the R154 conformation that supports the substrate ribose-phosphate backbone (Figure 3D). Therefore, the structural and mutagenesis data suggest that deprotonation of N3 is most likely mediated indirectly, potentially through

564 a water-assisted pathway. This interpretation is consistent with computational work on Nep1, in which
565 water-mediated proton shuttling to D101 was favored [48]. Taken together, our findings provide insight
566 into the catalytic mechanism of an unconventional methyltransferase with both similarities and
567 differences to Nep1.

568 The current study has also raised intriguing questions about the biological significance of the
569 H69 modifications. Helix 69 is a universally conserved and highly modified structural element located
570 near the decoding center between A- and P-site tRNAs and participating in intersubunit association,
571 whose key role presumably relies on its dynamics during translation. Modifications have been shown to
572 affect H69 dynamics in model RNAs [11–14] . Notably, it was reported that Ψs stabilize H69 under low pH
573 conditions [11], this is in agreement with increased doubling time of the *rlmH* and *rluD* double deletion
574 strain when grown at sub-optimal pH (Figure 5 B and C). Since increased doubling times were also
575 experienced by the *rlmH* single deletion strain, the corresponding methylation also seems to contribute
576 to bacterial fitness under acidic stress. Aside from H69 model RNAs, here we show that modifications
577 contribute to H69 conformation and dynamics in the context of the 70S ribosome (Figure S4). The
578 increased cold sensitivity of the *rlmH* single and *rlmH/rluD* double deletion strains (Figure 5 A and B)
579 implies that the modifications contribute to H69 dynamics during translation and, consequently, to
580 bacterial fitness.

581 ## Methods

582 ### *Strains and plasmids*

583 Generation of *rlmH* knockout (*ΔrlmH; rlmH* gene replaced with kanamycin resistance cassette)
584 and *rlmH/rluD* double knockout (*ΔrlmH/ΔrluD; rlmH* gene and *rluD* gene replaced with kanamycin and
585 chloramphenicol resistance cassettes, respectively) of *E. coli* MG1655 [27] strain is described in [21].
586 Notably, since the absence of the RluD enzyme strongly impairs cellular growth in *E. coli* K12-derived
587 strains [15], the *rluD/rlmH* double deletion strain was constructed using a so-called "pseudorevertant" *rluD*
588 deletion strain with compensatory mutations in the *prfB* gene. The *ΔrluD* pseudorevertant strain has a

589 WT-like growth phenotype despite lacking a functional RluD enzyme and the Ψs in H69 [17]. The *E. coli*
590 MG1655 strain was used for the wild-type control.

591 For this study, we constructed *rlmH* gene variants with mutations corresponding to substitutions
592 Y23A, E56A, L72A, D73A, G103A, E106A, G107A, S121A, L122A, T126A, L127A, P128A, H129A,
593 E138A, Y141A, R142A, R142L, R142K, Y152A, Y152F, H153A, and R154A in RlmH protein. PCR
594 was used for site-directed mutagenesis. Construction of the mutant RlmH protein expression vectors
595 based on the pBAD/*Myc*-HisC vector (Thermo Fisher Scientific, Life Technologies) was similar to the
596 wild-type RlmH expression vector (pBAD-*rlmH*) reported in [25]. For protein expression and purification
597 for structural studies, we used the pNIC28-Bsa4 vector (Addgene). Restriction endonucleases and other
598 enzymes for DNA manipulations were used according to the manufacturer's recommendations. Standard
599 techniques were used for DNA manipulation and plasmid DNA isolation [49]. Constructed plasmids were
600 verified by sequencing.

601 ***RlmH purification***

602 For structural studies, the pNIC28-Bsa4-*rlmH* vector, which introduces a TEV-cleavable N-
603 terminal His-tag to recombinant RlmH, was transformed into *E. coli* BL21(DE3) Rosetta chemo-
604 competent cells for protein expression. A single colony was selected and cultured in 2xYT media
605 supplemented with 50 µg/ml kanamycin until OD_{600} ~0.7. Protein expression was induced with 0.2 mM
606 isopropyl-β-d-thiogalactopyranoside (IPTG), and cells were grown with continuous shaking at 16 °C
607 overnight. Cells were harvested by centrifugation (4000 g for 10 min at 4°C) and resuspended in lysis
608 buffer (50 mM Tris/HCl, pH 7.5, 300 mM NaCl, 2 mM $MgCl_2$, 5% glycerol, and 1 mM DTT)
609 supplemented with DNase I (20 U/ml) and 1x Protease Inhibitor Cocktail. Cells were lysed by sonication
610 and centrifuged at 20 000 rpm for 30 min. at 4 °C. The supernatant was collected and incubated with
611 pre-equilibrated nickel–nitrilotriacetic acid (NTA) beads at 4 °C for 1 hour on a multi-rotator. The bound
612 protein was then purified by gravity-flow chromatography, with three washes using lysis
613 buffer containing 30 mM imidazole, followed by elution with 250 mM imidazole. Fractions were
614 concentrated using a 10-kDa molecular weight cutoff (MWCO) concentrator (Millipore) and loaded
615 onto a Superdex 200 16/600 gel filtration column (Cytiva) pre-equilibrated with buffer (50 mM

Tris/HCl pH 7.5, 300 mM NaCl, 5% glycerol, and 1 mM DTT). The target fractions were concentrated and snap-frozen for storage at -80 °C.

For *in vitro* methylation studies, native RlmH protein was purified from *E. coli* TOP10 (Invitrogen Life Sciences) cells, and mutant RlmH proteins from the rlmH knockout strain harboring the corresponding pBAD/Myc-HisC plasmids were grown in 2xYT media in the presence of 100 μg/ml ampicillin and 10 mM arabinose. Protein purification procedures using Q-Sepharose anion-exchange and SP-Sepharose cation-exchange chromatography are described in [25] and were based on RlmH methyltransferase activity. Concentration of mutant proteins was assessed relative to native RlmH using SDS-PAGE and ImageQuant software (GE Healthcare Life Sciences).

Ribosome purification

5 liters of 2xYT media supplemented with kanamycin (50 μg/ml) were incubated with overnight cultures of *E. coli* ΔrlmH and ΔrlmH/ΔrluD strains, and the cultures were grown at 37 °C with continuous shaking to an OD600 of ~0.5. Bacterial culture was cooled down on ice for 30 min., and cells were collected by centrifugation (3500 rpm for 20 min. at 4 °C). The cell pellet was washed with lysis dilution buffer (10 mM Tris/HCl pH 8.0, 60 mM KCl, 60 mM NH_4Cl, 12 mM $MgCl_2$, and 6 mM beta-mercaptoethanol), collected (8000 rpm for 15 min at 4 ºC), and resuspended in lysis buffer (50 mM Tris/HCl pH 8.0, 60 mM KCl, 60 mM NH_4Cl, 6 mM $MgCl_2$, 16% sucrose, and 6 mM beta-mercaptoethanol) supplemented with lysozyme (~1 mg/ml), DNase I (20 U/ml), RNase inhibitor (1 U/μl), and 1x Protease Inhibitor Cocktail. Cells were lysed by 4 cycles of freeze/thaw. Cell lysate was clarified by centrifugation (10 000 rpm for 30 min. at 4°C) and filtration using 0.44 μm syringe filters. ~100 A_{260} units of cell lysate was layered onto a 10-30% sucrose gradient in OV-10 buffer (10 mM Tris/HCl, pH 8.0, 60 mM KCl, 60 mM NH_4Cl, 10 mM $MgCl_2$, and 6 mM beta-mercaptoethanol) and centrifuged using the SW28 rotor at 19,000 rpm for 19 hours at 4°C. The ribosome profile was determined by continuous absorbance monitoring at 254 nm, and fractions were collected using a fractionation system (Brandel). Fractions corresponding to 70S ribosomes were pooled together, concentrated, and buffer-exchanged to buffer G (5 mM HEPES/KOH pH 7.5, 50 mM KCl, 10 mM NH_4Cl, 10 mM Mg-acetate, and 6 mM beta-mercaptoethanol) using 100 kDa cut-off centrifugation

643 filters (Amicon). 70S concentration was determined using Nanodrop A_{260} (1 unit corresponds to 23
644 picomoles of 70S). Ribosome quality was assessed by negative staining electron microscopy, and
645 ribosome samples were flash-frozen in liquid nitrogen and stored at -80 °C.

646 ***Negative staining electron microscopy***

647 The 70S sample (~ 0.2 A_{260} units/ml in buffer G) was applied to glow-discharged continuous
648 carbon film-coated 200-mesh copper grids (CF200-CU, Electron Microscopy Sciences). Following 1
649 min. of incubation, the sample was blotted by filter paper (Whatman). Then, 2% uranyl acetate was
650 added to the grid, incubated for 1 min, and gently blotted with filter paper. The grid was air-dried for 10
651 min. and loaded into a Tecnai T12 (FEI) instrument equipped with a 4K Eagle charge-coupled device
652 (CCD) camera.

653 ***RlmH-ribosome complex formation***

654 Recombinant (with N-terminal His-tag) native and mutant RlmH proteins (final concentration
655 5 μM), pre-incubated for 10 min. on ice with S-adenosyl homocysteine (SAH; f.c. 100 μM), were
656 incubated (final reaction volume 100 μl) with *ΔrlmH* or *ΔrlmH/ΔrluD* 70S ribosomes (f.c. 0.5 μM) in
657 buffer G (5 mM HEPES/KOH pH 7.5, 10 m Mg-acetate, 50 mM KCl, 10 mM NH_4Cl, and 6 mM β-
658 mercaptoethanol) at 37°C for 10 min. The sample was filtered using Spin-X (Corning Costar) centrifuge
659 filters and layered onto a 100 μl 1.1 M sucrose cushion in buffer G. Samples were pelleted by
660 centrifugation at 95,000 rpm for 1.5 hours at 4°C using an MLA-130 fixed-angle rotor (Beckman
661 Coulter). Pellets were washed and re-suspended in buffer G. Aliquots were taken, and protein
662 composition was analyzed by polyacrylamide gel electrophoresis using NuPAGE Bis-Tris 4-12% gel
663 (Thermo Fisher Scientific) and MES buffer (Thermo Fisher Scientific).

664 ***Cryo-EM data collection, processing, and model building***

665 The reconstituted RlmH(WT)-SAH-70S(*rlmH/rluD*) sample was applied to glow-discharged
666 Quantifoil 1.2/1.3 grids coated with 2 nm carbon and flash-frozen as described in [50]. Data was collected
667 on a Titan Krios (Thermo Fisher Scientific) 300 kV electron microscope equipped with a GIF Quantum

energy filter and a K3 direct electron detector (Gatan) with a defocus range between -0.6 µm and -1.2 µm. Movies were acquired at the magnification of 130 kx with a pixel size of 0.97 Å.

The movies were subjected to patch motion correction, followed by patch CTF estimation using CryoSPARC4.7 [51]. Micrographs with an estimated CTF resolution higher than 4 Å were selected for subsequent processing. A subset of particles was picked by the Blob Picker to generate 2D templates by 2D classification. Subsequently, 3D models for good and junk particles were generated by *ab-initio* reconstruction. Particles picked by the template picker were manually curated and extracted with box size 480. All the particles were subjected to three rounds of heterogeneous refinement to remove the contaminants and bad particles. After homogeneous refinement, particles were subjected to reference-based motion correction and local and global refinement. Masked 3D classification against RlmH separates 70S ribosomes into RlmH-bound (70S-RlmH) and RlmH-free states. RlmH-free 70S ribosomes were further separated into three states: vacant 70S, 70S bound with P-tRNA (70S-P), and 70S bound with both A- and P-tRNA (70S-AP). Particles of all 70S states were subjected to final non-uniform refinement. The resulting maps for vacant 70S, 70S-P, 70S-AP, and 70S-RlmH were resolved at 2 Å, 2.42 Å, 2.84 Å, and 2.19 Å, respectively, based on gold-standard Fourier shell correlation (FSC) = 0.143.

The models of the 70S ribosome (PDB ID: 8BF7) and RlmH (PDB ID: 5TWK) were manually fitted to the maps in ChimeraX [52]. All models were subjected to Phenix real-space refinement and manually refined in COOT [53,54]. Figures were generated using ChimeraX and PyMol.

In vivo methylation assay

For the *in vivo* methylation assay, the *rlmH* and *rlmH/rluD* deletion strains were transformed with vectors (pBAD-based) encoding wild-type or mutant RlmH proteins. Standard transformation methods with ampicillin for colony selection were used [49]. 400 ml of 2xYT media supplemented with ampicillin (100 µg/ml) and kanamycin (25 µg/ml) was inoculated with overnight bacterial cultures and incubated on a shaker at 37°C. 4x100 ml cultures were collected between OD_{600} ~ 0.3 and ~ 2.4. In parallel, 100 ml of 2xYT media supplemented with the antibiotics was inoculated and incubated on a

shaker until OD_{600} ~ 0.2. Protein expression from the plasmid was started with the addition of arabinose (0.002%), and cells were further incubated until OD_{600} = 2.0. Alternatively, cells with mutant RlmH expression vectors were grown with (+ara) or without (-ara) arabinose induction until OD600 ~2.5. Cells were pelleted with low-speed centrifugation at 4°C. Expression level of RlmH protein variants was assessed by analyzing total protein expression on a 15% polyacrylamide/SDS gel electrophoresis run for 2.5 hours at 200V in Tris-glycine buffer.

Ribosomes and rRNA were prepared as described in [21]. Shortly, 70S ribosomes from the *in vivo* methylation assay were collected using sucrose density centrifugation, ribosomes were precipitated with ethanol, and rRNA for primer extension analysis was extracted using PN buffer (Qiagen) as described in [4].

Primer extension analysis using the U1 primer (CAG CCT GGC CAT CAT TAC GCC), complementary to the positions 1972-1992 of *E. coli* 23S rRNA, and separation of cDNAs using polyacrylamide/urea gel electrophoresis were carried out as described in [21]. Gel was transferred to Whatman 3MM paper and vacuum dried. Radioactivity was visualized using Typhoon PhosphorImager (GE Healthcare). Quantification of bands corresponding to the stop signal induced by m3-pseudouridine 1915 was performed using ImageJ.

In vitro methylation assay

For *in vitro* methylation assays, 70S ribosomes were isolated from the *rlmH* deletion strain grown in 2xYT media supplemented with kanamycin (25 μg/ml) until OD_{600} ~ 0.7. The in vitro activity of the mutant RlmH proteins was characterized by determining their kinetic parameters. Methylation buffer (50 mM Tris/HCl, pH 8.0, 100 mM NH4Cl, 10 mM MgCl2, and 1 mM DTT) and suboptimal RlmH protein concentrations (0.07-0.35 M, depending on the mutant) were used for kinetic assays. To determine the apparent K_M for substrate 70S ribosomes, 100 mM [^{3}H]-SAM (PerkinElmer) and mutant RlmH proteins were pre-incubated for 10 min at 37°C in 25 μl. [^{3}H]-methyl group incorporation was measured after addition of 0.5–4.3 mM (final volume 50 μl) 70S ribosomes (isolated from *rlmH* deletion strain) and incubation for 20/40/60 sec. at 37 °C. For the determination of the apparent K_M for cofactor

SAM, 10–75 mM [^{3}H]-SAM and RlmH were pre-incubated for 10 min at 37°C. [^{3}H]-methyl group incorporation was measured after addition of 2 mM 70S ribosomes and incubation for 15/30/45 sec. at 37 °C. Reaction products were precipitated with TCA, and radioactivity was determined as described in [25]. The slopes of methyl group incorporation versus time plots were calculated, and the initial rates obtained were plotted against the respective substrate concentrations. From fitting the Michaelis-Menten equation to the data, apparent K_M and k_{cat} values were determined.

Growth assay

2 ml of LB media supplemented with relevant antibiotics was inoculated with single colonies of wild-type MG1655, *rlmH* (*ΔrlmH*), and *rlmH/rluD* (*ΔrlmH/ΔrluD*) deletion strains and grown at 37 °C with continuous shaking until mid-log phase. Cultures were diluted (OD_{600} ~ 0.01) to 200 µl/well of fresh LB or M9 minimal (pH 5.0, 7.0, and 9.0) media in 96-well suspension culture plates. If indicated, 0.5 M NaCl or 100 mM EDTA were added to LB media. No antibiotics were added. Alternatively, 10 µM or 50 µM viomycin or capreomycin was added. Plates were covered with a microplate lid and incubated at 37, 30, or 25 °C (with continuous shaking at 140 rpm). OD_{580} was determined using Tecan Spark^{TM} 10M every 10 min for up to 20 h. Doubling time (g) was calculated from the early log phase [$g = \ln 2/r$, where $r = \ln(N/N_0)/(t - t_0)$]. Average doubling times and standard deviations were calculated from at least two biological replicates with at least three technical replicates each.

Data availability

Cryo-EM maps and atomic models have been deposited in the Electron Microscopy Databank (EMD-XXXXX etc.) and Protein Databank (PDB ID: XXXX etc.). All other data are included in the manuscript and/or supporting information.

References

1. Ofengand, J., Del Campo, M. & Kaya, Y. Mapping Pseudouridines in RNA Molecules. *Methods* **25**, 365–373 (2001).
2. Decatur, W. A. & Fournier, M. J. rRNA modifications and ribosome function. *Trends in Biochemical Sciences* **27**, 344–351 (2002).

3. Wiechert, F. *et al.* Visualizing the modification landscape of the human 60S ribosomal subunit at close to atomic resolution. *Nucleic Acids Research* **53**, gkae1191 (2025).
4. Liiv, A., Karitkina, D., Maiväli, Ü. & Remme, J. Analysis of the function of E. coli 23S rRNA helix-loop 69 by mutagenesis. *BMC Molecular Biol* **6**, 18 (2005).
5. Hennelly, S. P. *et al.* A Time-resolved Investigation of Ribosomal Subunit Association. *Journal of Molecular Biology* **346**, 1243–1258 (2005).
6. Schuwirth, B. S. *et al.* Structures of the Bacterial Ribosome at 3.5 Å Resolution. *Science* **310**, 827–834 (2005).
7. Kowalak, J. A. *et al.* Structural Characterization of U*-1915 in Domain IV from Escherichia Coli 23S Ribosomal RNA as 3-Methylpseudouridine. *Nucleic Acids Research* **24**, 688–693 (1996).
8. Raychaudhuri, S., Conrad, J., Hall, B. G. & Ofengand, J. A pseudouridine synthase required for the formation of two universally conserved pseudouridines in ribosomal RNA is essential for normal growth of Escherichia coli. *RNA* **4**, 1407–1417 (1998).
9. Charette, M. & Gray, M. W. Pseudouridine in RNA: What, Where, How, and Why. *IUBMB Life* **49**, 341–351 (2000).
10. Meroueh, M. Unique structural and stabilizing roles for the individual pseudouridine residues in the 1920 region of Escherichia coli 23S rRNA. *Nucleic Acids Research* **28**, 2075–2083 (2000).
11. Jiang, J., Kharel, D. N. & Chow, C. S. Modulation of conformational changes in helix 69 mutants by pseudouridine modifications. *Biophysical Chemistry* **200–201**, 48–55 (2015).
12. Desaulniers, J.-P. *et al.* Pseudouridines in rRNA helix 69 play a role in loop stacking interactions. *Org. Biomol. Chem.* **6**, 3892 (2008).
13. Jiang, J., Aduri, R., Chow, C. S. & SantaLucia, J. Structure modulation of helix 69 from *Escherichia coli* 23S ribosomal RNA by pseudouridylations. *Nucleic Acids Research* **42**, 3971–3981 (2014).
14. Sakakibara, Y. & Chow, C. S. Role of Pseudouridine in Structural Rearrangements of Helix 69 During Bacterial Ribosome Assembly. *ACS Chem. Biol.* **7**, 871–878 (2012).
15. Gutgsell, N. S., Deutscher, M. P. & Ofengand, J. The pseudouridine synthase RluD is required for normal ribosome assembly and function in *Escherichia coli*. *RNA* **11**, 1141–1152 (2005).

16. Clark, Z. S. & O'Connor, M. Suppressor analysis links trans-translation and ribosomal protein uS7 to RluD function in Escherichia coli. *Biochemical and Biophysical Research Communications* **700**, 149584 (2024).
17. O'Connor, M. & Gregory, S. T. Inactivation of the RluD Pseudouridine Synthase Has Minimal Effects on Growth and Ribosome Function in Wild-Type *Escherichia coli* and *Salmonella enterica*. *J Bacteriol* **193**, 154–162 (2011).
18. Chui, H. M.-P., Meroueh, M., Scaringe, S. A. & Chow, C. S. Synthesis of a 3-methyluridine phosphoramidite to investigate the role of methylation in a ribosomal RNA hairpin. *Bioorganic & Medicinal Chemistry* **10**, 325–332 (2002).
19. Chui, H. M.-P., Desaulniers, J.-P., Scaringe, S. A. & Chow, C. S. Synthesis of Helix 69 of *Escherichia c oli* 23S rRNA Containing Its Natural Modified Nucleosides, m^3 Ψ and Ψ. *J. Org. Chem.* **67**, 8847–8854 (2002).
20. Purta, E., Kaminska, K. H., Kasprzak, J. M., Bujnicki, J. M. & Douthwaite, S. YbeA is the m^3 Ψ methyltransferase RlmH that targets nucleotide 1915 in 23S rRNA. *RNA* **14**, 2234–2244 (2008).
21. Ero, R., Peil, L., Liiv, A. & Remme, J. Identification of pseudouridine methyltransferase in *Escherichia coli*. *RNA* **14**, 2223–2233 (2008).
22. Tkaczuk, K. L., Dunin-Horkawicz, S., Purta, E. & Bujnicki, J. M. Structural and evolutionary bioinformatics of the SPOUT superfamily of methyltransferases. *BMC Bioinformatics* **8**, 73 (2007).
23. Schubert, H. L., Blumenthal, R. M. & Cheng, X. Many paths to methyltransfer: a chronicle of convergence. *Trends in Biochemical Sciences* **28**, 329–335 (2003).
24. Sordyl, D. *et al.* MODOMICS: a database of RNA modifications and related information. 2025 update and 20th anniversary. *Nucleic Acids Research* **54**, D219–D225 (2026).
25. Ero, R., Leppik, M., Liiv, A. & Remme, J. Specificity and kinetics of 23S rRNA modification enzymes RlmH and RluD. *RNA* **16**, 2075–2084 (2010).
26. Nikolay, R. *et al.* Snapshots of native pre-50S ribosomes reveal a biogenesis factor network and evolutionary specialization. *Molecular Cell* **81**, 1200-1215.e9 (2021).

27. Leppik, M., Ero, R., Liiv, A., Kipper, K. & Remme, J. Different sensitivity of H69 modification enzymes RluD and RlmH to mutations in Escherichia coli 23S rRNA. *Biochimie* **94**, 1080–1089 (2012).
28. Siibak, T. & Remme, J. Subribosomal particle analysis reveals the stages of bacterial ribosome assembly at which rRNA nucleotides are modified. *RNA* **16**, 2023–2032 (2010).
29. Koh, C. S., Madireddy, R., Beane, T. J., Zamore, P. D. & Korostelev, A. A. Small methyltransferase RlmH assembles a composite active site to methylate a ribosomal pseudouridine. *Sci Rep* **7**, 969 (2017).
30. Wurm, J. P. *et al.* The ribosome assembly factor Nep1 responsible for Bowen–Conradi syndrome is a pseudouridine-N1-specific methyltransferase. *Nucleic Acids Research* **38**, 2387–2398 (2010).
31. Meyer, B. *et al.* The Bowen–Conradi syndrome protein Nep1 (Emg1) has a dual role in eukaryotic ribosome biogenesis, as an essential assembly factor and in the methylation of Ψ1191 in yeast 18S rRNA. *Nucleic Acids Research* **39**, 1526–1537 (2011).
32. Thomas, S. R., Keller, C. A., Szyk, A., Cannon, J. R. & LaRonde-LeBlanc, N. A. Structural insight into the functional mechanism of Nep1/Emg1 N1-specific pseudouridine methyltransferase in ribosome biogenesis. *Nucleic Acids Research* **39**, 2445–2457 (2011).
33. Chatterjee, K. *et al.* The archaeal COG1901/DUF358 SPOUT-methyltransferase members, together with pseudouridine synthase Pus10, catalyze the formation of 1-methylpseudouridine at position 54 of tRNA. *RNA* **18**, 421–433 (2012).
34. Basturea, G. N. & Deutscher, M. P. Substrate specificity and properties of the *Escherichia coli* 16S rRNA methyltransferase, RsmE. *RNA* **13**, 1969–1976 (2007).
35. Strassler, S. E., Bowles, I. E., Dey, D., Jackman, J. E. & Conn, G. L. Tied up in knots: Untangling substrate recognition by the SPOUT methyltransferases. *Journal of Biological Chemistry* **298**, 102393 (2022).
36. Ito, T. *et al.* Structural basis for methyl-donor-dependent and sequence-specific binding to tRNA substrates by knotted methyltransferase TrmD. *Proc Natl Acad Sci U S A* **112**, E4197-4205 (2015).

828 37. Selmer, M. *et al.* Structure of the 70 *S* Ribosome Complexed with mRNA and tRNA. *Science* **313**,
829 1935–1942 (2006).
830 38. Anantharaman, V., Koonin, E. V. & Aravind, L. SPOUT: a class of methyltransferases that
831 includes spoU and trmD RNA methylase superfamilies, and novel superfamilies of predicted
832 prokaryotic RNA methylases. *J Mol Microbiol Biotechnol* **4**, 71–75 (2002).
833 39. Elkins, P. A. *et al.* Insights into Catalysis by a Knotted TrmD tRNA Methyltransferase. *Journal of*
834 *Molecular Biology* **333**, 931–949 (2003).
835 40. Lee, N., Francklyn, C. & Hamilton, E. P. Arabinose-induced binding of AraC protein to araI2
836 activates the araBAD operon promoter. *Proc. Natl. Acad. Sci. U.S.A.* **84**, 8814–8818 (1987).
837 41. Ehrenberg, M., Bremer, H. & Dennis, P. P. Medium-dependent control of the bacterial growth
838 rate. *Biochimie* **95**, 643–658 (2013).
839 42. Bremer, H. & Dennis, P. P. Modulation of Chemical Composition and Other Parameters of the
840 Cell at Different Exponential Growth Rates. *EcoSal Plus* **3**, 10.1128/ecosal.5.2.3 (2008).
841 43. Woodruff, L. B. A. *et al.* Genome-scale identification and characterization of ethanol tolerance
842 genes in Escherichia coli. *Metabolic Engineering* **15**, 124–133 (2013).
843 44. Treede, I. *et al.* The avilamycin resistance determinants AviRa and AviRb methylate 23S rRNA at
844 the guanosine 2535 base and the uridine 2479 ribose. *Molecular Microbiology* **49**, 309–318
845 (2003).
846 45. Thompson, J., Schmidt, F. & Cundliffe, E. Site of action of a ribosomal RNA methylase
847 conferring resistance to thiostrepton. *J Biol Chem* **257**, 7915–7917 (1982).
848 46. Stanley, R. E., Blaha, G., Grodzicki, R. L., Strickler, M. D. & Steitz, T. A. The structures of the
849 anti-tuberculosis antibiotics viomycin and capreomycin bound to the 70S ribosome. *Nat Struct*
850 *Mol Biol* **17**, 289–293 (2010).
851 47. Grosjean, H., Edqvist, J., Stråby, K. B. & Giegé, R. Enzymatic Formation of Modified
852 Nucleosides in tRNA: Dependence on tRNA Architecture. *Journal of Molecular Biology* **255**, 67–
853 85 (1996).

48. Jedrzejewski, M. *et al.* Nucleolar Essential Protein 1 (Nep1): Elucidation of enzymatic catalysis mechanism by molecular dynamics simulation and quantum mechanics study. *Comput Struct Biotechnol J* **21**, 3999–4008 (2023).
49. Green, M. R. & Sambrook, J. *Molecular Cloning: A Laboratory Manual*. (Cold Spring Harbor laboratory press, Cold Spring Harbor, 2012).
50. Go, K. D. *et al.* Antimalarial drug artemisinin stabilizes PfRACK1 binding to the ribosome. *Structure* **33**, 1386-1397.e5 (2025).
51. Punjani, A., Rubinstein, J. L., Fleet, D. J. & Brubaker, M. A. cryoSPARC: algorithms for rapid unsupervised cryo-EM structure determination. *Nat Methods* **14**, 290–296 (2017).
52. Pettersen, E. F. *et al.* UCSF CHIMERAX : Structure visualization for researchers, educators, and developers. *Protein Science* **30**, 70–82 (2021).
53. Adams, P. D. *et al. PHENIX* : a comprehensive Python-based system for macromolecular structure solution. *Acta Crystallogr D Biol Crystallogr* **66**, 213–221 (2010).
54. Emsley, P., Lohkamp, B., Scott, W. G. & Cowtan, K. Features and development of *Coot*. *Acta Crystallogr D Biol Crystallogr* **66**, 486–501 (2010).

Acknowledgements

This work was supported by Tier I grants (RG RG34/24, RT24/23) from the Ministry of Education (MOE) of Singapore, and Singapore National Research Foundation (NRF) Competitive Research Programme (CRP) grant NRF-CRP27-2021RS-0001 (Y.-G.G.), and by the Estonian Ministry of Education and Research (PUT PRG1179 to J.R.).

Author contributions

Y.-G.G. and J.R. conceived and designed this study; E.R., Y.Y.J, D.P.H., and A.L. conducted the experiments; Y.X.-F. and S.S. acquired and analyzed the data; R.E., J.R., and Y.-G.G. drafted the manuscript and all authors read and edited the manuscript.

Funding

We disclose the support for the research of this work from the following funders: Ministry of Education – Singapore (MOE) grants RG34/24 and RT24/23 (Y.-G.G.), National Research Foundation Singapore (NRF) grant NRF-CRP27-2021RS-0001 (Y.-G.G.), and Estonian Ministry of Education and Research grant PUT PRG1179 (J.R.).

Competing interests

The authors declare no competing interests.

Tables and figures

Table 1. Kinetic parameters of RlmH variants.

RlmH	K_M (70S) µM	k_{cat} (70S) min^{-1}	k_{cat}/K_M (70S) $min^{-1}/µM$	K_M (SAM) µM	k_{cat} (SAM) min^{-1}	k_{cat}/K_M (SAM) $min^{-1}/µM$
WT[a]	0.51 ± 0.06	4.95 ± 1.10	9.71	27 ± 3	6.41 ± 1.32	0.24
WT	0.29 ± 0.03	4.76 ± 0.90	16.41	25 ± 3	6.32 ± 1.03	0.25
L72A				36 ± 4	6.71 ± 1.11	0.19
D73A				39 ± 3	6.9 ± 0.92	0.18
G103A				41 ± 4	6.57 ± 0.85	0.16
E106A	0.95 ± 0.08	1.77 ± 0.12	1.86			
G107A	0.38 ± 0.03	4.22 ± 0.22	11.11	52 ± 6	4.73 ± 0.76	0.09
S121A				29 ± 3	6.39 ± 0.77	0.22
L122A				33 ± 3	7.1 ± 1.44	0.22
T126A	1.09 ± 0.09	3.69 ± 0.27	3.39			
H129A	1.32 ± 0.09	4.46 ± 0.50	3.38			
E138A	8.25 ± 0.50	8.93 ± 1.32	1.08			
R142A	1.82 ± 0.09	3.3 ± 0.8	1.81			
R142K	2.67 ± 0.27	3.14 ± 0.7	1.18			
Y152F	0.19 ± 0.03	1.05 ± 0.09	5.53			
H153A	0.37 ± 0.04	2.24 ± 0.07	6.05			
R154A	0.37 ± 0.03	1.43 ± 0.07	3.86			

The amount of [^{3}H]-methyl groups incorporated was monitored by acid precipitation and scintillation counting. Initial rates of the methylation reaction were calculated from the time-courses of the product formation at different substrate or co-factor concentrations, and Michaelis-Menten equation was used to determine the kinetic parameters.

[a] from ref. [25]

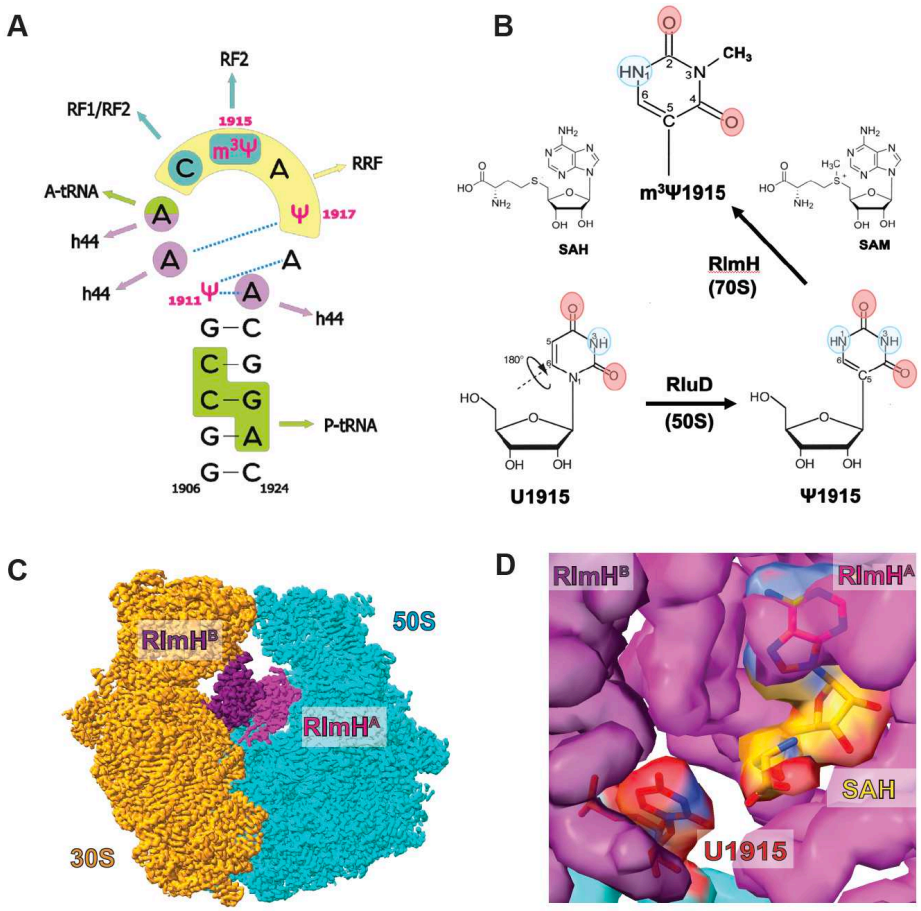
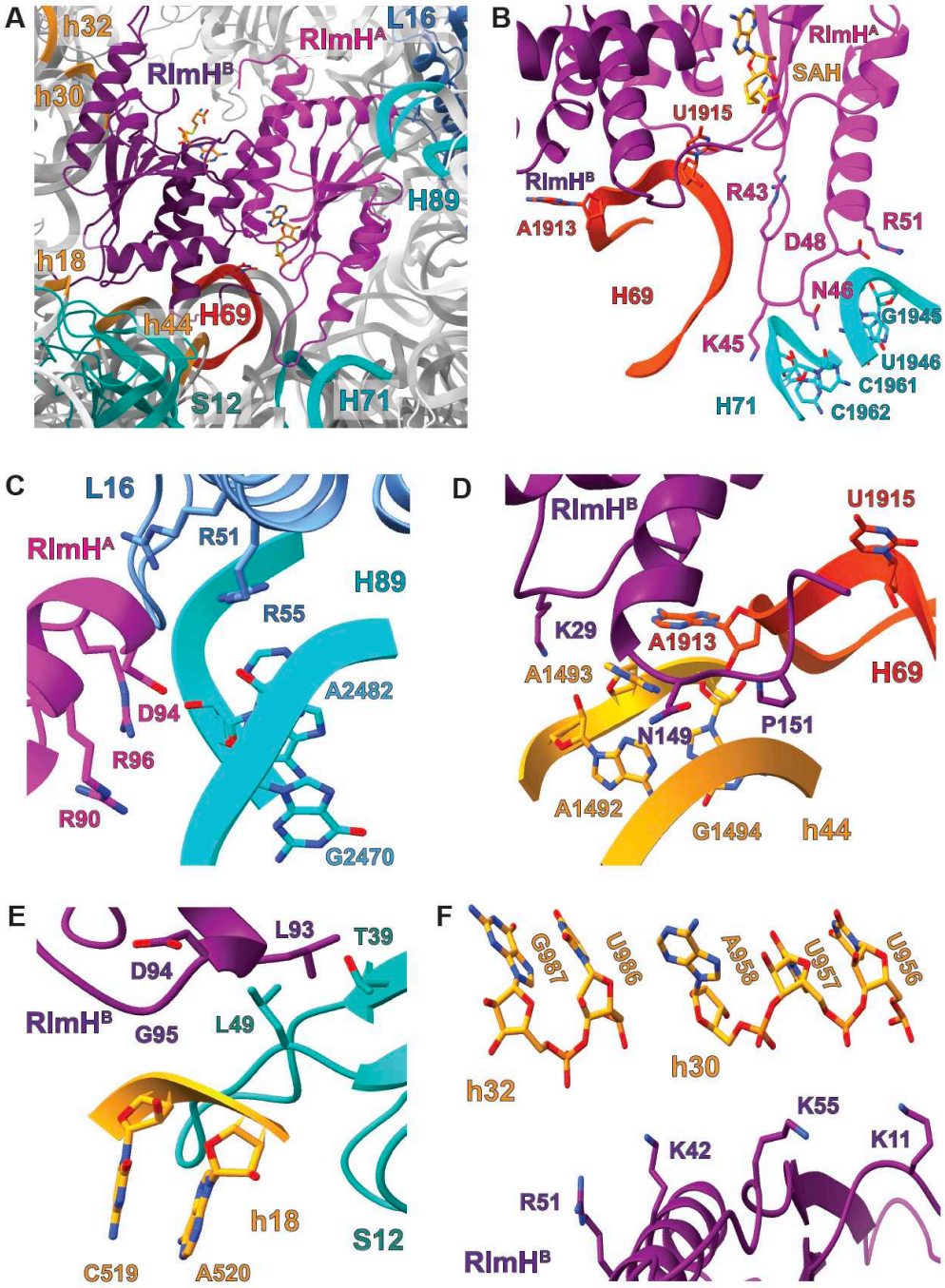


Figure 1. RlmH is the N3-specific methyltransferase that modifies pseudouridine 1915 in H69 in 70S ribosomes. A) The sequence and secondary structure of the *E. coli* 23S rRNA H69 showing key interactions within H69 itself, with 16S rRNA helix 44 (h44), A- and P-site tRNAs, and protein factors (RFs and RRF). Pseudouridine and N3-methylpseudouridine are marked with Ψ and $m^3Ψ$, respectively. Tertiary interactions within H69 are indicated by dotted blue lines. H69 contacts with A- and P-site tRNAs, h44, release factors (RFs), and ribosome recycling factor (RRF) are shown by arrows. **B)** The two-step synthesis pathway of $m^3Ψ1915$. First, the pseudouridine synthase RluD isomerizes uridine 1915 (as well as uridines 1911 and 1917) to pseudouridine in nearly mature 50S subunits. Then, RlmH binds to 70S ribosomes and catalyzes the methyl group transfer from cofactor SAM to the N3 nitrogen in pseudouridine, resulting in $m^3Ψ1915$ and SAH. Hydrogen bond donor (blue) and acceptor (red) sites in bases are highlighted. **C)** Cryo-electron microscopy electron density map of the *ΔrlmH/ΔrluD* 70S ribosomes with electron density in the A-site corresponding to the RlmH dimer. Protomer A (magenta) and B (purple) interact predominantly with the 50S and 30S subunits, respectively. **D)** Electron density corresponding to the U1915 base and the SAH in the catalytic site.



910

911 **Figure 2. RlmH interactions with the ribosome. A)** Overview of RlmH dimer interactions with 50S
912 (shown in cyan) and 30S (shown in yellow) rRNA regions and the r-proteins L16 (light blue) and S12
913 (orange). Detailed interactions with the H69 loop region (red) will be discussed later. **B)** Close-up view
914 of RlmH protomer A ($RlmH^A$) interaction with H71. **C)** Close-up view of $RlmH^A$ interaction with H89
915 and the r-protein L16. **D)** Close-up view of $RlmH^B$ interaction with h44. **E)** Close-up view of $RlmH^B$
916 interaction with h18 and the r-protein S12. **F)** Close-up view of $RlmH^B$ interaction with h30 and h32.
917 Key residues are shown in sticks and labeled.

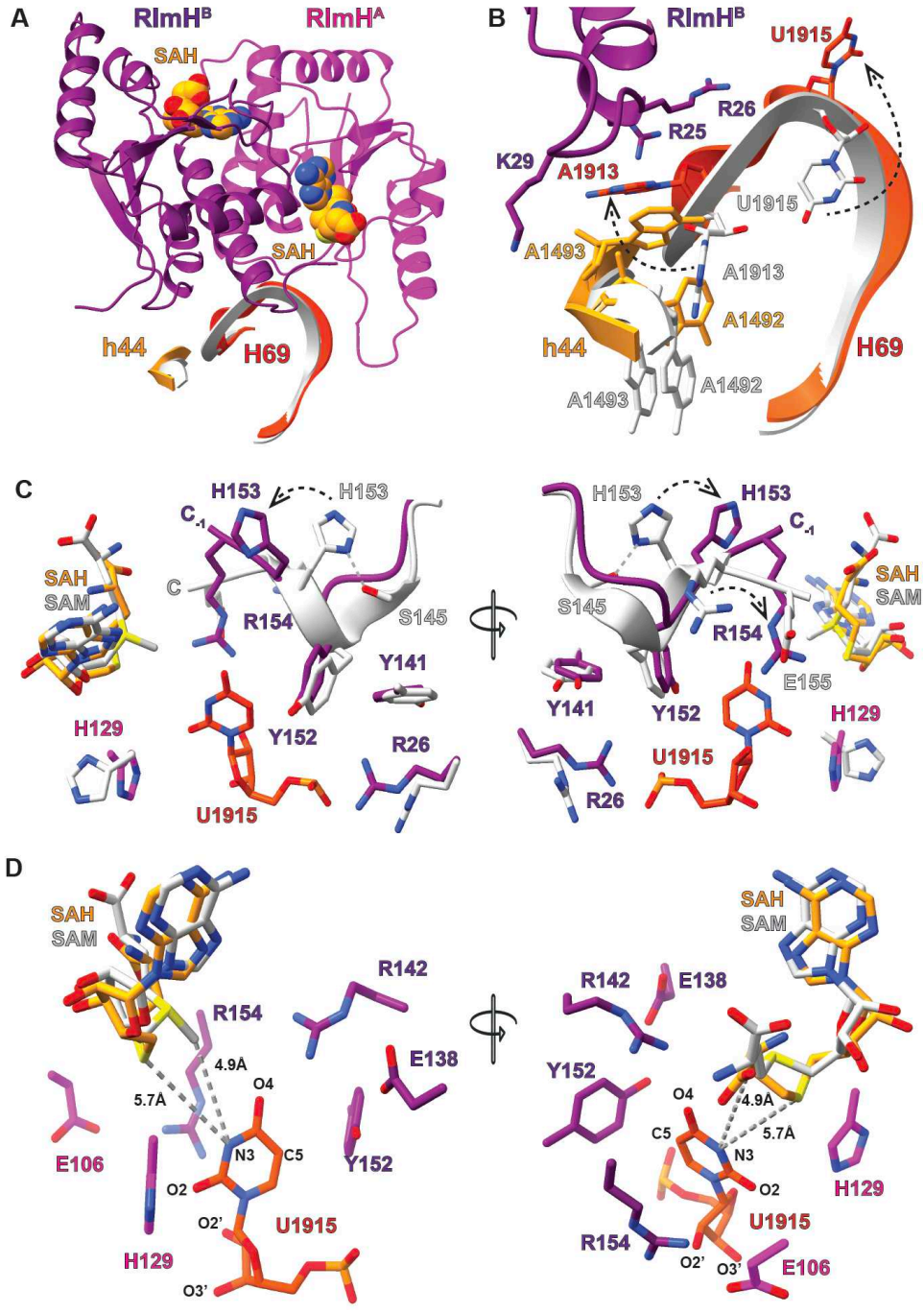
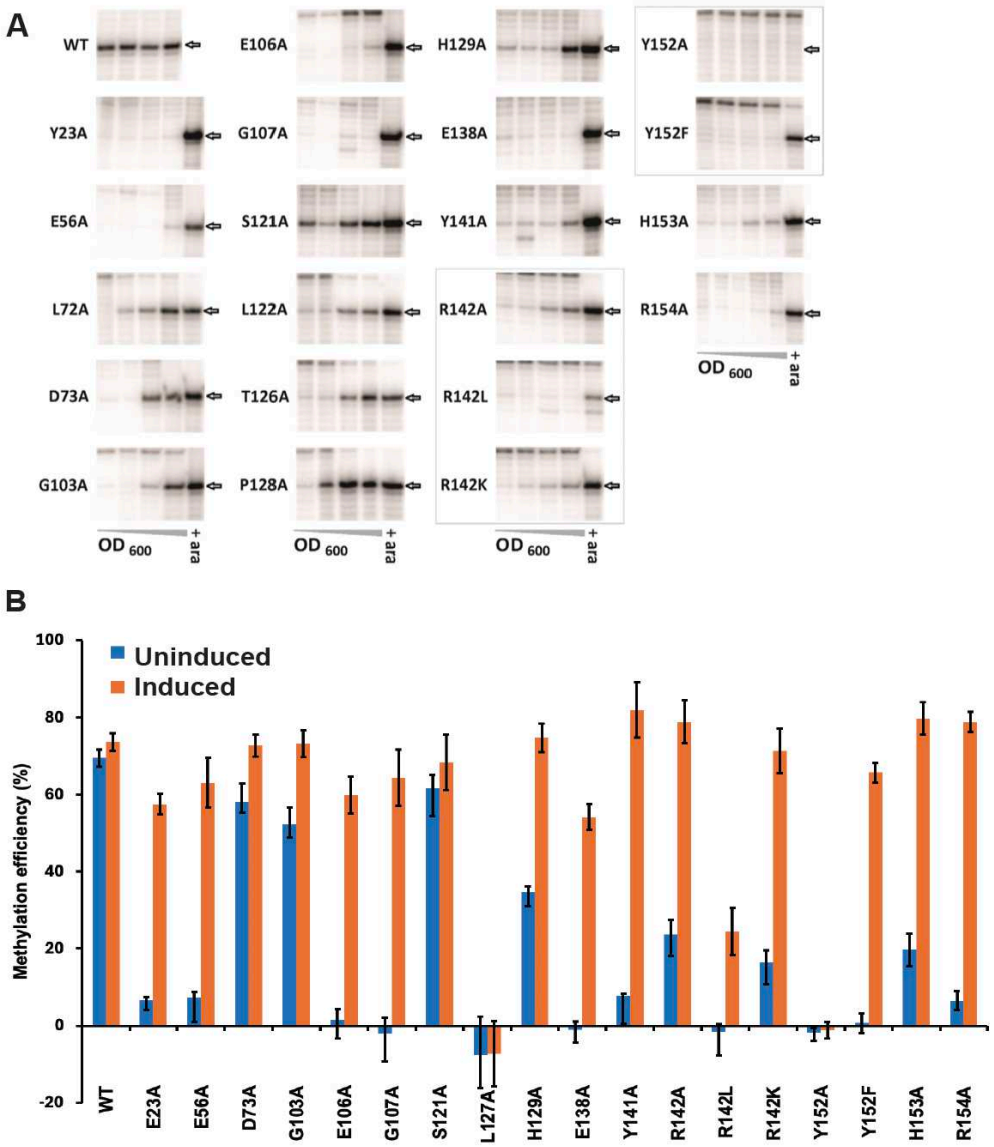


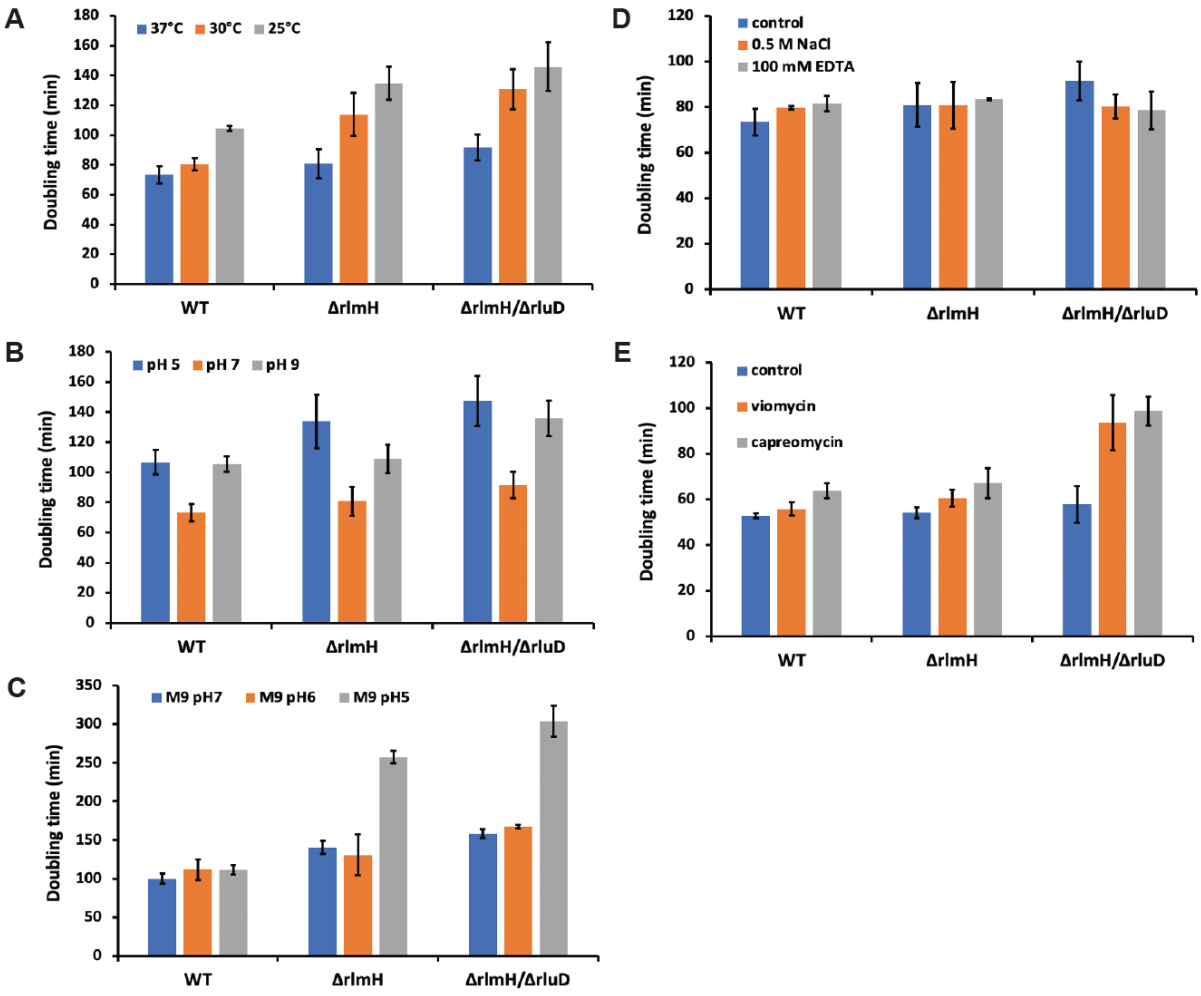
Figure 3. Conformational changes in the substrate H69/h44 region, the catalytic site, and RlmH residues involved in substrate base binding and catalysis. Overall **A)** and a close-up view **B)** of RlmH-binding-induced conformational changes in H69 U1915 and A1913 compared to the vacant *ΔrlmH/ΔrluD* 70S ribosome shown in gray. **B)** The U1915 "base flipping" movement and the rotation of the A1913 towards RlmH are shown with arrows. The corresponding changes in h44 residues A1492, and A1493 are shown as well. The $RlmH^B$ residues involved in the stabilization are shown in sticks and labeled. **C)** Different views of the substrate-binding-dependent conformational changes in the RlmH-

SAH catalytic site. RlmH-SAM crystal structure (PDB: 5TWJ [29]) is shown in gray for comparison. The RlmH residues undergoing notable conformational change are shown in sticks, labeled, and highlighted by arrows. **D)** Different views of the catalytic site. RlmH residues involved in substrate base binding and stabilization are shown in sticks and labeled. SAH is from the current structure; SAM is modeled based on the RlmH-SAM crustal structure. Corresponding distances between the methyl group donor and acceptor sites are shown**.**



933

934 **Figure 4. The effect of mutations on RlmH activity *in vivo*. A)** Formation of $m^3\Psi$1915 in *E. coli rlmH*
935 deletion strain expressing low or moderate amounts (+ara) of native (WT) and mutant RlmH proteins
936 was monitored. rRNA was extracted from ribosomes of cells collected from different growth phases
937 (OD_{600} 0.3-2.4). Reverse transcriptase-dependent primer extension analysis followed by separation of
938 cDNAs on urea-PAGE was used to detect $m^3\Psi$1915. The stop signal corresponding to $m^3\Psi$1915 is
939 indicated by an arrow. A representative of two independent experiments is shown. **B)** Quantification of
940 $m^3\Psi$1915 in late log phase (OD_{600} ~2.5) *E. coli rlmH* deletion strain expressing low (uninduced; -
941 arabinose, leaky expression) or moderate (induced; + arabinose) levels of wild-type and mutant RlmH
942 proteins.



943

944 **Figure 5. Physiological significance of H69 modification under stress conditions.** The effect of *rlmH*
945 and *rlmH/rluD* deletion on *E. coli* growth at suboptimal conditions compared to the wild-type strain. **A)**
946 Doubling times when grown in LB medium (pH 7) at 37 °C, 30 °C, and 25 °C. **B)** Doubling times when
947 grown in LB medium with pH 5, pH 7, and pH 9 at 37 °C. **C)** Doubling times when grown in M9
948 medium with pH 5, pH 7, and pH 9 at 37 °C. **D)** Doubling times when grown in LB medium (pH 7)
949 supplemented with 0.5 M NaCl or 100 mM EDTA at 37 °C. **E)** Doubling times when grown in LB
950 medium (pH 7) at 37 °C in the presence of 50 µg/ml viomycin or capreomycin supplemented.

951

Supplementary Files

This is a list of supplementary files associated with this preprint. Click to download.

- 44IJ.pdf
- 44II.pdf
- 44EW.pdf
- RlmHNaturecommSI.pdf
- 44IK.pdf
- NCOMMS26090985rs.pdf
- nrreportingsummaryfilled17942872802.pdf